 CMC, vol.11, no.1, pp.33-58, 2009

Hydroplaning Analysis for Tire Rolling over Water Film with Various Thicknesses Using the LS-DYNA Fluid-Structure Interactive Scheme

Syh-Tsang Jenq[1,2] **and Yuen-Sheng Chiu**[2]

Abstract: Current work studies the transient hydroplaning behavior of 200 kPa inflated pneumatic radial tires with various types of tread patterns. Tires were numerically loaded with a quarter car weight of 4 kN, and then accelerated from rest rolling over a water film with a thickness of 5, 10 and 15 mm on top of a flat pavement. Tire structure is composed of outer rubber tread and inner fiber reinforcing composite layers. The Mooney-Rivlin constitutive law and the classical laminated theory (CLT) were, respectively, used to describe the mechanical behavior of rubber material and composite reinforcing layers. The tire hydroplaning phenomenon was analyzed by the commercial finite element code - LS-DYNA. The Arbitrary Lagrangian & Eulerian (ALE) formulation was adopted to depict the fluid-structure interaction (FSI) behavior. Three different tire tread patterns, i.e. the smooth (blank) tread pattern and the 9 and 18 mm wide longitudinally-grooved tread patterns, were constructed to perform the current transient hydroplaning analysis. Simulated dynamic normal contact force and hydroplaning velocity of tire with a prescribed smooth tread pattern were obtained. The computed results were in good agreement with the numerical and test results given by Okano, et al. (2001) for tire running over 10 mm thick water fluid film. In addition, dynamic contact force of a smooth tread pattern tire rolling on a dry flat pavement was also found to be close to the result reported by Nakajima, et al. (2000). In addition, the effect of fluid water layer thickness on the hydroplaning velocity and normal contact force for tires with smooth tread pattern and longitudinally-grooved tread patterns rolling on a wet roadway analyzed by the LS-DYNA code are reported and discussed.

Keywords: radial tire, rolling contact analysis, hydroplaning, smooth tread pattern, longitudinal grooved tread pattern, composite material

[1] Corresponding author. E-mail: stjenq@mail.ncku.edu.tw, Fax: +886-6-2083641.
[2] Department of Aeronautics & Astronautics, National Cheng Kung University, No. 1, University Rd., Tainan, 70101, Taiwan, R.O.C.

1 Introduction

When a car is moving on the roadway, rubber tread is the part that interacts with the road surface. Since various types of tread patterns are available for commercial tires, the dry and wet contact rolling conditions may generally affect the steering and braking capability of the vehicle. Therefore, it seems important to study the effect of tread patterns on the dynamic response of tire rolling on a dry or wet pavement. It is a complicated fluid-structure interaction (FSI) problem to analyze the tire with a specific tread pattern rolling over a water fluid film on a road surface numerically.

Limited researches using the finite element method (FEM) to solve the current coupled tire rolling and hydroplaning problem were located. In 2000, Nakajima et al [Nakajima et al (2000)] used a commercial FEM code - DYTRAN to analyze the rolling and hydroplaning contact behavior of advanced pneumatic tires. The normal contact force between tire tread pattern and road surface was reported. This complex hydroplaning analysis of tires with smooth and practical tread patterns were presented. They showed that tire with the practical tread pattern has better hydroplaning characteristics than the smooth (blank) tread tire. In addition, they also reported that the nose angle of the tread pattern of the practical tire may increase the hydroplaning characteristics.

Grogger and Weiss [Grogger H., Weiss M. (1996)] used the finite volume method (FVM) to simulate the three-dimensional free surface fluid flow and also construct a smooth tread pattern tire FEM model. Three driving velocities of 30, 60 and 90 km/hr were applied to their analytic model. The pressure distribution of water flow, lift and drag forces, and drag coefficient were clearly presented in this paper. In addition, their experimental results were consistent to the calculated pressure distributions. For a driving speed of 90 km/hr case, poor agreement was reported because pressure loading deviated from measured values, and this may due to the fact that the tire deformation during hydroplaning was not accounted. Moreover, Grogger and Weiss [Grogger and Weiss (1997)] utilized the similar method to analyze hydroplaning behavior of smooth and longitudinally-grooved tread pattern tires. In this paper, it showed that the tire with longitudinally-grooved pattern owns better hydroplaning characteristics than that with smooth tread pattern for a driving speed of 30, 60 and 90 km/hr. The deformation of tread pattern was also reported to be a critical point that may influence on the hydroplaning velocity. The simulated results were in good agreement with their experimental data.

T. Okano and M. Koishi [Okano and Koishi (2001)] also used the explicit FEM code - DYTRAN to model and analyze the complicated hydroplaning problem. Four types of tread pattern, i.e., smooth, longitudinal, V-shaped and newly proto-

type pattern, were chosen in the rolling and hydroplaning analysis. The normal contact force and hydroplaning velocity were numerically determined and compared with experimental results. The tire with the longitudinally-grooved tread pattern possesses higher hydroplaning velocity than the tire with smooth (blank) tread pattern.

A simplified analysis of the tire-tread contact problem has been carried out in an attempt to predict deformation as well as stresses at different critical sections of tire tread section using the displacement potential based finite-difference technique [Reaz Ahmed and Deb Nath (2009)]. Both the qualitative and quantitative results as well as the comparison with the usual computational method firmly establish the reliability as well as superiority of the results, which are thus expected to be of great help for accurate and economic design of tires. Two re-entrant corners of the tread shoulder section are identified to be the most critical regions in terms of stresses; otherwise, the overall stress level at the contact boundary is higher than that of any other sections in the tread. Furthermore, both material properties and geometrical parameters of the tread section would have significant influence on the service life of treads, as the frictional resistance required from the road surface to keep the contact boundary free from lateral slippage is found to depend on them substantially.

Tire standing wave was reported [An and Cho (2008)] to be one of the crucial factors that may lead to unexpected tire structural failure because the total strain energy of the tire dramatically increases when it occurs. Its analytical analysis has been limited owing not only to the complicated tire structure and material composition, but also to the problem nonlinearity. In this paper, its characteristics are numerically investigated with the help of the transient dynamic rolling analysis of the 3-D patterned tire model. However, references (5) and (6) do not report the hydroplaning behavior of tires.

The present tire rolling and hydroplaning FEM analysis utilizes the commercial LS-DYNA code to analyze the present fluid-structure coupled FEM model. Simulated dynamic normal contact force and hydroplaning velocity of tire with a prescribed smooth tread pattern are to be compared with the results by Okano, et al. (2001). In addition, the dynamic contact force of a smooth tread pattern tire rolling on a dry flat pavement is also to be determined and then check against with the results reported by Nakajima, et al. (2000). The adequacy and accuracy of the present coupled FEM rolling and hydroplaning model can be assured if the current simulated results are found to be in a good agreement with the previous test findings and numerical results.

In the present FEM modeling, it is emphasized on studying the effect of smooth and 9 and 18 mm longitudinally-grooved tread pattern tires rolling and hydroplan-

ing on a road surface with a 5, 10 and 15 mm thick water fluid film. Notice that the viscous effect of water fluid film was considered in the present ALE coupled FEM analysis with the single-material and void (SMV) meshes defined. Tire structure is composed of outer rubber tread and inner fiber reinforcing composite layers. The Mooney-Rivlin constitutive law and the classical laminated theory (CLT) were, respectively, used to describe the mechanical behavior of rubber material and composite reinforcing layers. In order to be computationally efficient in the current coupled FEM analysis, shell elements were adopted here instead of using the solid elements [Jenq et al (2008)] for mesh construction of the inner tire composite material zones. Therefore, the transient rolling and hydroplaning response of a 4,000 N car weight loaded tire (195/65/R15) with a smooth and 9 mm narrow and 18 mm wide longitudinal-grooved tread patterns are studied in this work. Effect of the fluid water layer thickness on the hydroplaning characteristics of tires studied is to be reported and discussed. The dynamic contact and hydroplaning responses of tires rolling from the rest on a dry/wet and flat pavement are reported. Notice that the roadway and water fluid film were accelerated from rest to 120 km/hr numerically. The friction induced traction load was transferred to tire in order to roll over the water film with a thickness of 5, 10 and 15 mm on top of the flat pavement. Notice that the static and dynamic coefficients of friction between tire and roadway were set to be unity in the present study.

2 Tire structure and hydroplaning fluid film models

The radial inflated tires with a simple smooth tread pattern and two types of the longitudinally-grooved tread patterns were studied here. The transient hydroplaning behavior of 200 kPa inflated 195/65R15 radial tires with various types of tread patterns is studied in this work. Tires were numerically loaded with a quarter car weight of 4 kN. Roadway and the water fluid film were accelerated to 120 km/hr, the static and dynamic coefficients of friction between the roadway and tire were set to be unity in order to transfer the traction load to the tire which may roll over the water film with a thickness of 5, 10 and 15 mm on top of the flat pavement. The commercial finite element Code - LS-DYNA and the Hypermesh preprocessor were used to model and analyze the present radial tires made of rubber, steel reinforcing wires and fiber reinforcing composite layer materials. Basically, tire is composed of external rubber tread, sidewall rubber and internal reinforcing layers, such as the inner liner, carcass, steel belt, bead filler and bead wires.

The Mooney-Rivlin constitutive law was adopted in the current coupled FEM analysis in order to describe the non-linear elastic behavior of rubber, and the classical laminated theory (CLT) was also used to depict the mechanical stress-strain behavior of the fiber reinforced composite layers. A schematic representation of the

cross-sectional profile of tire studied is shown in Fig. 1. The effective elastic moduli of the fiber reinforcing layers shown in Fig. 1 were obtained [Gibson (2007); Jenq et al (2008)] for the current FEM analysis. Because the tire structure is quite complicated, we subdivided the tire structure into eleven composite material subregions in order to distinguish their unique composite layout. Fig. 2 shows the arrangement of these eleven different composite material zones for the subsequent finite element tire rolling and hydroplaning analysis.

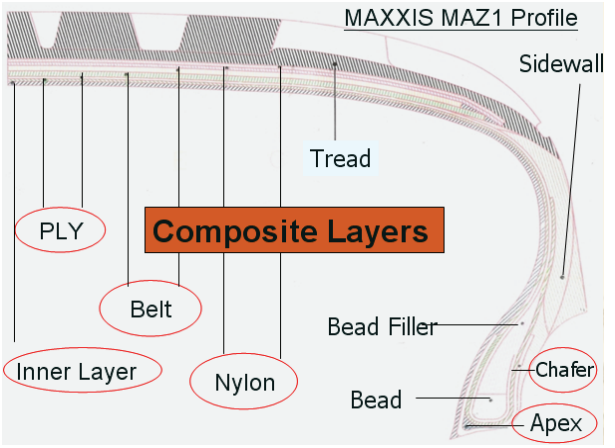

Figure 1: A schematic representation of the cross-sectional view of the tire studied.

Based on the cross-sectional view graph shown in Fig. 2, the shell elements were used to construct the tire's inner composite layers located under rubber tread and sidewall of tire in order to reduce the degree of freedom and also the computational cost for the present rolling and hydroplaning FEM analysis. Fig. 3 reveals that the inner tire composite materials sub-regions 1 to 7 (i.e. zone comp1 to comp7) were numerically constructed by shell finite elements. However, the external tire tread, sidewall, bead and chafer were modeled by the hexahedron and pentahedron solid elements in order to construct the specific tread patter and sidewall shape as requested. Note that these solid elements which correspond to outer tire materials sub-regions 8 to 11 (i.e. zone comp8 to comp11) and external rubber material regions (i.e. tread, sidewall) are presented in Fig. 4. Sidewall and tire tread were composed of synthesized rubber material, and the Mooney-Rivlin nonlinear constitute law was adopted to described their mechanical response. Fig. 5 shows a schematic plot of tire rolling on the dry and flat pavement. According to the coordinate system shown in Fig. 5, the x-, y- and z-direction contact forces between the tire and pavement correspond, respectively, to the lateral, tractive and normal

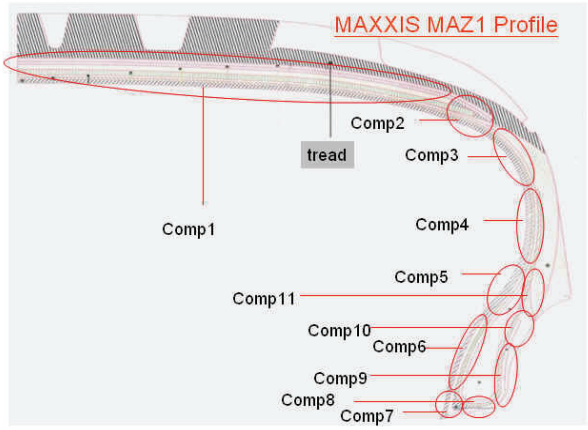

Figure 2: Arrangement and layout of the 11 composite material zones for the current radial tire.

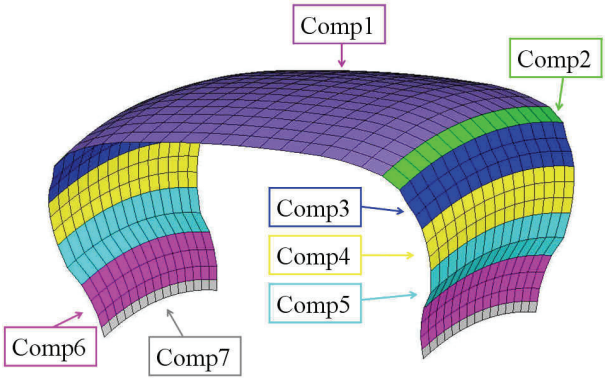

Figure 3: Finite element meshes of tire's internal shell elements constructed which was composed of the layered composite material for zone 1 to 7.

contact forces exerted to the inflated radial tire.

In the present work, the tire hydroplaning phenomenon was analyzed by the commercial finite element code - LS-DYNA. The Arbitrary Lagrangian & Eulerian (ALE) formulation was adopted to depict fluid-structure interaction (FSI) behavior. Three different tire tread patterns, i.e. the smooth (blank) tread pattern and the 9mm and 18 mm longitudinally-grooved width tread patterns, were numerically constructed in order to perform the transient rolling and hydroplaning coupled FEM analysis. The simulated dynamic normal contact force and the hydroplaning

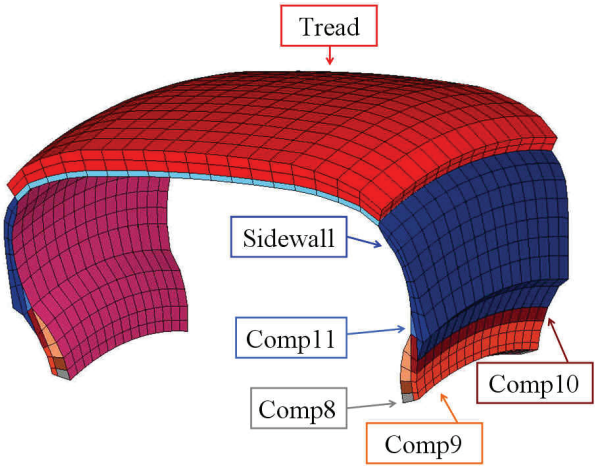

Figure 4: The finite element mesh plot for a section of tire's solid elements corresponding to materials zone 8 to 11 (i.e. zone comp8 to comp11).

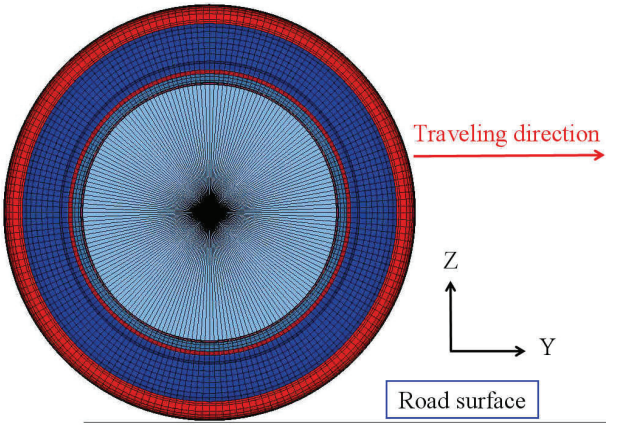

Figure 5: A schematic drawing of tire rolling on the dry and flat pavement.

velocity of tire with prescribed tread pattern are to be determined and discussed in the following sections.

Current FEM model for tire rolling and hydroplaning coupled analysis contains 109,560 hexahedron elements that were utilized to construct the water film and air void layers. Additional 28,800 Lagrangian 8-node hexahedron and 6-node pentahedron solid elements and 7,560 simplified reinforcing composite Belytschko-Tsay shell elements were constructed for the tire structure with smooth tire tread pattern

as shown in Fig 6(a). Fig. 6(b) and (c) show the FEM mesh models each containing a total of 36,000 solid and shell elements for the tire structure with 9 mm narrow and 18 mm wide longitudinally-grooved tread patterns. Furthermore, 6,354 quadrangle or triangle shell elements were constructed for the flat road surface structure and the rim of tire. It is noted that the mechanical behavior for both road and tire rim structures were assumed to behave as a rigid body in the current simulations. A complete finite element mesh plot which represents (1) the flat road surface, (2) the radial tire, and (3) the incoming water film and air void layer for rolling and hydroplaning coupled analysis is presented in Fig. 7.

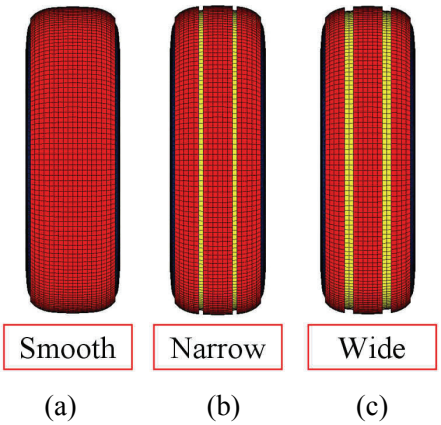

Figure 6: The FEM models of tires with (a) smooth (blank), (b) 9 mm narrow longitudinal-grooved and (c) 18 mm wide longitudinal-grooved tread patterns.

The convergence tests of the present finite element model were performed in order to assure the accuracy of the analyzed numerical results. Fig. 8(a) shows the relationship between the element number of tire model and the simulated tire hydroplaning velocity, when element number of the fluid film (containing the water film and air void layer) was set to be 109,560 as mentioned above. Furthermore, a plot of the fluid film element number versus the tire hydroplaning velocity is presented in Fig. 8(b), when the element number of tire model was chosen to be 36,360 as described in the previous paragraph. Upon examining Figures 8(a) and (b), it reveals that a converged numerical solution can be obtained when the element number of the present tire model and the fluid film model are, respectively, chosen to be more than 24,240 and 69,696 elements. However, a more refined tire and the fluid film numerical models with element number of 36,360 and 109,560 were respectively constructed for the current coupled finite element analysis.

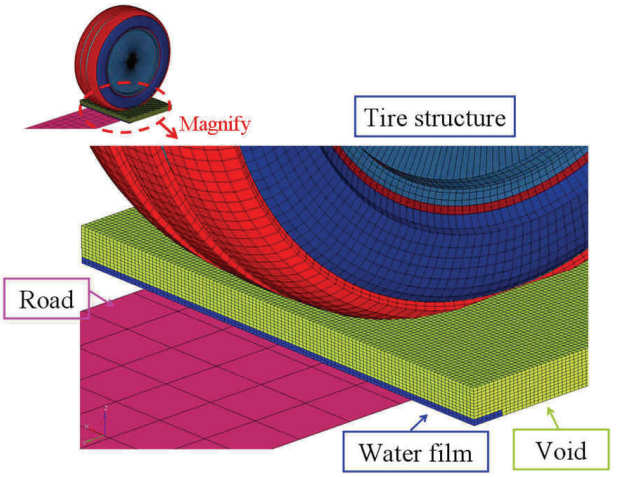

Figure 7: A complete finite element mesh plot which represents (1) the flat road surface, (2) the radial tire, and (3) the incoming water film and air void layer for rolling and hydroplaning coupled analysis.

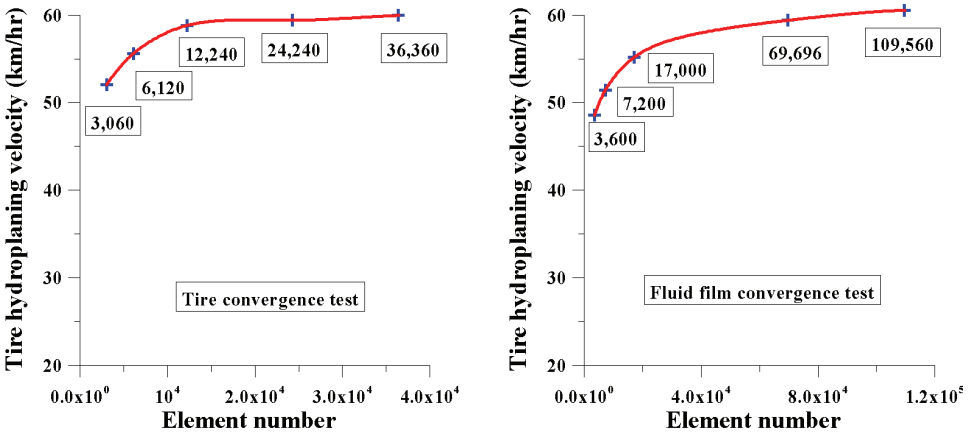

(a) (b)

Figure 8: Convergence tests of the present finite element model: (a) A relation between tire element number and tire hydroplaning velocity; and (b) a relation between fluid film element number and tire hydroplaning velocity in the present FEM analysis.

3 Dynamic rolling contact simulation & verification using a tire with blank tread pattern

In the present study, we emphasize on modeling and analyzing the dynamic contact behavior of inflated pneumatic tires rolling on a dry/wet flat pavement. In order to

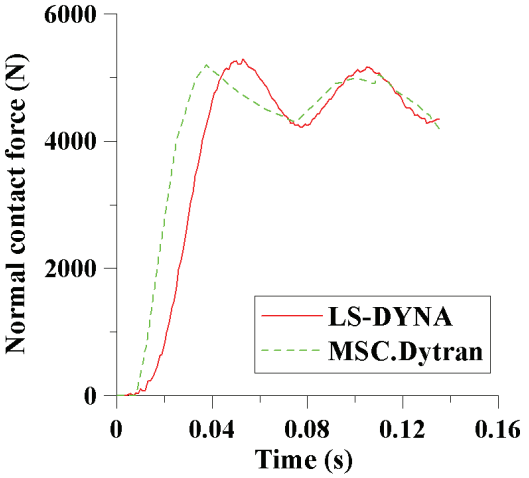

Figure 9: The relationship between time and normal contact force of blank (smooth) tread pattern tire.

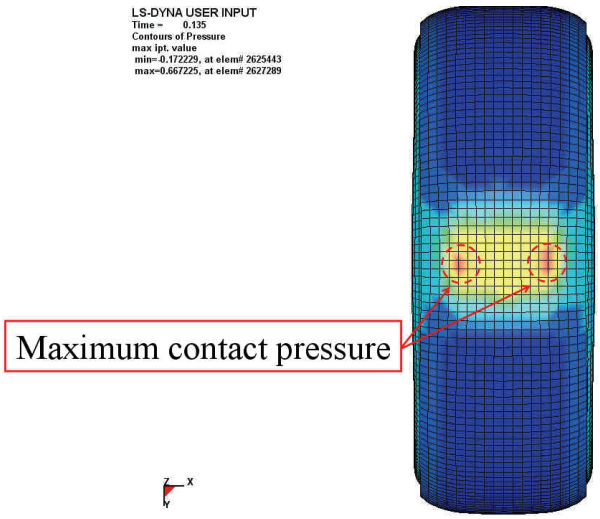

Figure 10: The maximum contact pressure contour plot of the tire contact region at time equals to 135 ms after inflation initiated.

assure the accuracy and adequacy of the current numerical analyzed results, it is necessary for us compare our numerical model simulated results with the reported results available in the literature. A previously published paper by Nakajima, et

al. [Nakajima et al (2000)] reported the time histories of contact forces of tire with blank tread pattern for a period of time before a section of tire with specific tread pattern rolling in contact with dry or wet road surface. We, therefore, re-performed the finite element analysis using LS-DYNA for the 205/55R16 radial tire with blank pattern rolling on a dry road surface as described in the work by Nakajima, et al. [Nakajima et al (2000)] According to Nakajima, et al. [Nakajima et al (2000)]'s work, the blank (smooth) tread tire was initially inflated to 220 kPa, and was rolling on a dry-flat roadway from rest to 60 km/hr. Note that the tire was loaded with a quarter car weight of 4,500 N during tire rolling process for 135 ms. The Hypermesh pre-processor in conjunction with the explicit LS-DYNA solver were used to construct the FEM numerical model for this 205/55R16 radial tire with blank pattern. In reference [1], the tire was inflated until 5 ms and a quarter car weight was loaded until 50 ms, then the rolling state was steadily accelerated from 50 ms to 135 ms. The tire reached a velocity of 60 km/hr till 135 ms on a dry flat pavement.

Based on above paragraph's descriptions, the FEM model of a 205/55R16 radial tire with blank (smooth) tread pattern was constructed and analyzed using the commercial LS-DYNA explicit code. Fig. 9 shows the relationship between the time and normal contact force of the tire in question. Solid line shown in Fig. 9 represents for the current LS-DYNA simulated results; while the dotted line shown in the figure was obtain from the result reported by Nakajima, et al. [Nakajima et al (2000)] using the MSC.Dytran. Upon examining these two curves shown in Fig. 9, it reveals that good relationship between the simulated normal contact force and time after load was applied for the 205/55R16 radial tire with blank (smooth) pattern. This close relationship seems to assure us that the present FEM model can be properly applied for the dynamic dry rolling contact analysis for radial tires.

Note that early stage transient response predicted by the present LS-DYNA model seems to be slightly different from the benchmark MSC.Dytran solution [Nakajima et al (2000)]. Similar to this benchmark model, both an initial tire inflating pressure of 220 kPa and a 4.5 kN initial car weight loading were, respectively, applied to the radial tire in 5 and 50 ms in the present numerical model. A linear loading relationship between the inflating pressure and time was used in the current analysis. In addition, a linear car weight loading was also applied to tire in the present work. Notice that the loading rate for tire inflating and car weight loading were not described in ref. (1). This may result in the early stage deviation between the present model predicted curve and the benchmark curve shown in Fig. 9. In addition, the rubber material properties used in reference (1) were not provided and the material constants used in the present study were given by the Cheng Shin Rubber Ind. Co. Ltd. The variation of material properties used in the finite element model

could also produce deviation between the present model predicted curve and the benchmark curve shown in Fig. 9.

Fig. 10 shows the region which the maximum contact pressure occurred on blank tread pattern tire when time is equal to 135 ms after inflation initiated. According to Fig. 10, the two peak pressure zones in the contact pressure field studied are located at the edges of the contact shoulder area. Notice that a similar appearance of the maximum peak contact pressure located in the contact area was reported by Ghoreishy [Ghoreishy (2006)] and Clark [Clark (1981)] for a radial tire under rolling condition.

4 Hydroplaning analysis verfication using blank (smooth) tread pattern tire

Since the hydroplaning phenomenon is a key issue related to safe driving on wet roadway, it would be convictive if the current LS-DYNA simulated results for the coupled tire rolling and fluid flow problem can be solved properly and accurately. Then we can proceed to investigate the other tire's hydroplaning characteristics with a specific tread pattern and/or the tire construction using the LS-DYNA commercial FEM coupled code.

The previous coupled 195/65R15 tire and fluid model reported by Okano and Koishi [Okano and Koishi (2001)] was chosen here to reconstruct their tire hydroplaning numerical model using the Hypermesh pre-processor and then to perform the coupled analysis by the LS-DYNA code. Therefore, the 200 kPa inflated 195/65R15 tire with blank (smooth) tread pattern rolling on a wet roadway vertically loaded with a quarter car weight of 4,000 N examined by Okano and Koishi [Okano and Koishi (2001)] was numerically studied here in order to check against their reported experimental result. Notice that in the present verification process the mechanical loading applied to the tire is composed of two stages. The first stage is to inflate and apply the 4,000 N quarter cart weight to the tire in 1 s numerically. The second stage is to accelerate tire from rest on the wet pavement to a specific speed in 0.12 sec. Thus, the total operational duration time for this numerical hydroplaning verification process is 1.12 sec.

A complete finite element mesh plot which represents the (1) flat road surface, (2) radial tire, and (3) incoming water film and air void layer for tire rolling and hydroplaning analysis is shown in Fig. 7. It is noted that during the tire's initial stage inflation and 4,000 N quarter car weight loadings, the fluid film/void layer elements will not interact with the deformed tire elements. Otherwise, it will not be consistent with the present scenario for the tire inflation, self-weight loading, and then rolling into the specified fluid film on a flat pavement to study the hydroplaning FEM analysis using the LS-DYNA code.

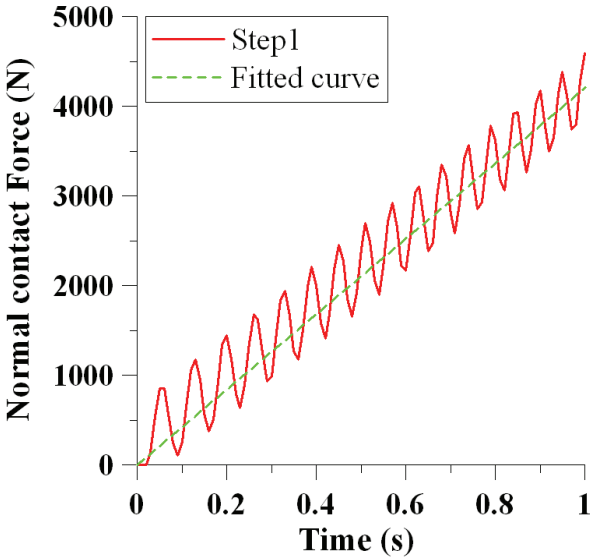

Figure 11: The relationship between normal contact force and duration time in the inflated process.

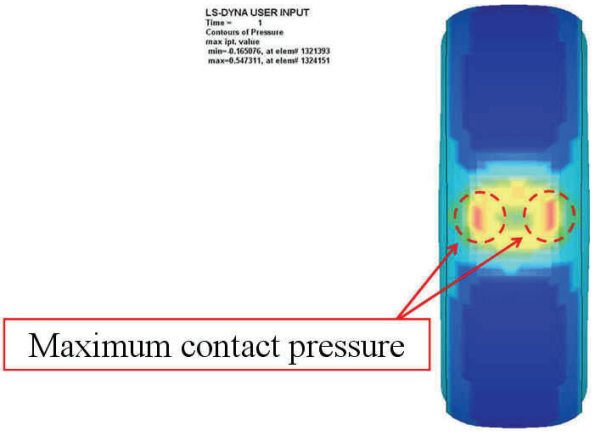

Figure 12: A plot about the area of maximum contact pressure on the contact region between the tire and road surface.

Fig. 11 shows the relationship between the simulated tire normal contact force and the time of the blank (smooth) tread tire inflated to 200 kPa in 1 sec. on a dry flat pavement. During the tire inflation stage, a quarter car weight of 4,000 N was

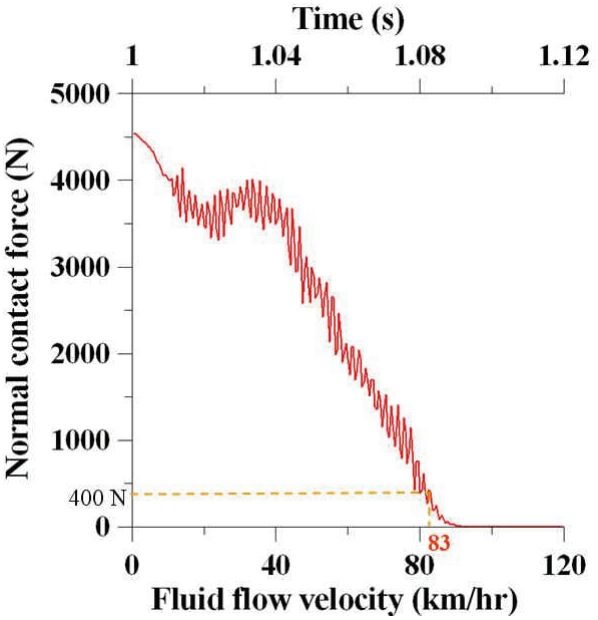

Figure 13: Relationship between the LS-DYNA simulated normal contact force and fluid flow velocity using the ALE formulation for the smooth tread pattern tire.

also applied to the tire. Fig. 11 shows that an oscillated normal contact force was observed due to the proposed ramp loading condition applied to the FEM solver. The contact force at time equal to 1 sec. (i.e. the end of inflation and car weight loading time) is determined to be approximately 4,351.3 N due to the mentioned inflation pressure loading and a quarter of car weight loading. The location of the maximum contact pressure was found to be near the tire shoulder section as shown in Fig. 12.

The scenario of the second stage can be described by a stationary inflated tire (with 4,000N car weight loaded) accelerated from the rest and rolls into the 10 mm thick water/void film pavement from 1s to 1.12sec. During simulation, the relative velocity of the road and the water layer to tire are increased from zero initially to 120 km/hr at the end with a constant acceleration in 0.12 sec. of physical time. Using the relationships between fluid flow velocity and contact force that are thus obtained, one can determine the desired "hydroplaning velocity." Notice that the "hydroplaning velocity" in the simulation was defined [Okano and Koishi (2001)] as the transverse velocity at which the contact force between the tire and road surface drop to 10% of the tire load. The Arbitrary Lagrangian & Eulerian (ALE) formula-

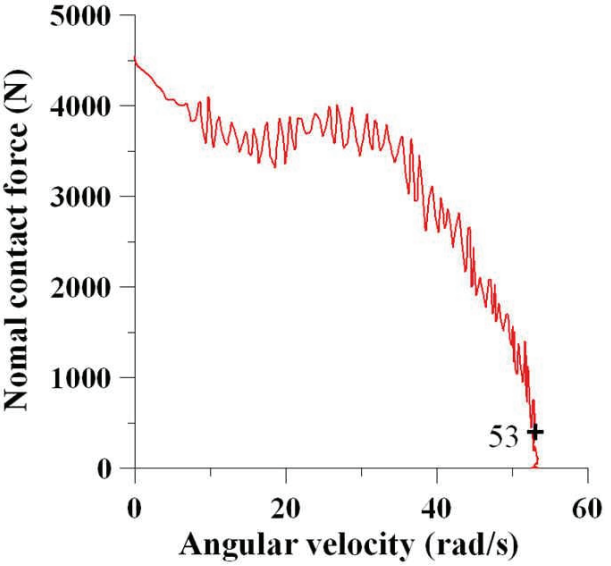

Figure 14: The relationship between LS-DYNA simulated normal contact force and angular velocity of wheel rim by using the coupled FEM analysis of a smooth tread pattern radial tire.

tion available in the LS-DYNA code which governs the fluid-structure interaction (FSI) phenomenon were used for the current coupled water film/void layer and tire rolling analysis. Fig. 13 shows the relationship between normal contact force and fluid flow velocity simulated by using ALE formulation for the pneumatic tire with smooth pattern. When fluid flow velocity is approximately greater than 38 km/hr, Fig. 13 shows that the simulated normal contact force between the tire and wet road surface decreases abruptly. This is resulted from the fact that the contact region between tire and roadway decreases due to the intrusion of fluid water layer. When the flow velocity is near 83 km/hr, the normal contact force between the smooth tread pattern tire and the wet pavement is determined to be approximately 400 N (i.e., 10% of the tire load). Therefore, the corresponding hydroplaning velocity of this tire is numerically determined to be near 83 km/hr. Furthermore, figure 14 shows the relationship between the simulated normal contact force and the angular velocity of wheel rim by using the coupled LS-DYNA analysis of a smooth tread pattern radial tire. The hydroplaning velocity defined above can be related to a specific tire traveling velocity if the relationship between the normal contact force and the angular velocity of wheel rim is determined, as shown in Fig. 14. Therefore, when a tire travels with a velocity of 60.6 km/hr, the hydroplaning phenomenon

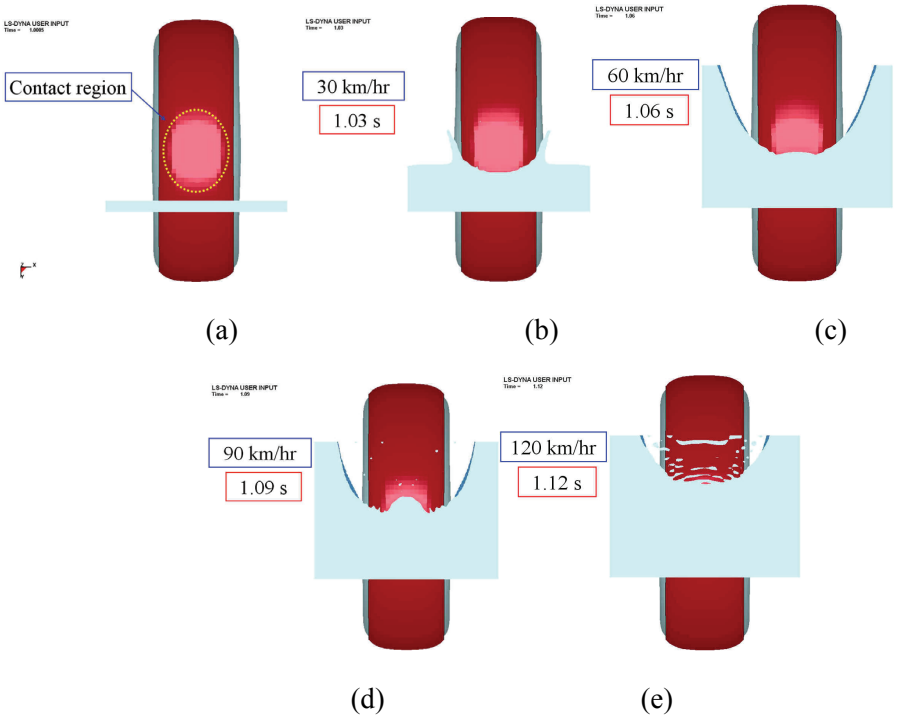

Figure 15: The bottom view of the simulated splashing graphs for the blank pattern tire rolling over a water film when tire was accelerated from rest to a speed of (a) contact region (b) 30 km/hr, (c) 60 km/hr, (d) 90 km/hr, and (e) 120 km/hr.

may occur. Notice that a tire velocity of 60.6 km/hr is derived by multiplying the rim angular velocity of 53 rad/s shown in Fig. 14 with the tire radius of 317.25 mm (measured from the original center of the rim to the external tire tread surface).

Figs. 15 show the bottom view of the simulated splashing graphs for the blank pattern tire rolling over a 10 mm thick water film when the fluid flow speed equals to (a) 30 km/hr (0.03 s after acceleration initiated) and (b) 60 km/hr (0.06 s after acceleration initiated) and (c) 90 km/hr (0.09 s after acceleration initiated) and (d) 120 km/hr (0.12 s after acceleration initiated). Fig. 15(a) shows that the tire is about to roll into the 10 mm thick water/void film, and the (dry) contact region is presented inside the dotted circle. Fig. 15(b) shows that the tire rolls into the water film with a flow velocity of 30 km/hr (0.030 s after tire entering the water film) and water film on the roadway is pushed sideway and also splashes by the smooth tread pattern tire. When fluid flow velocity is accelerated to 60 km/hr (0.060 s after tire entering the water film) as shown in Fig. 15(c), it shows that more water

intrudes into the interface between tire smooth tread and road surface. According to Fig. 15(c), the area of tire contact region decreases due to the intrusion of water film. Fig. 15(d) shows that the contact area between tire tread and road surface is furthermore reduced when tire fluid flow velocity is increased to 90 km/hr (0.090 s after tire entering the water film). Notice that the above mentioned hydroplaning velocity of the current studied tire was determined to be 83 km/hr. Because the fluid flow velocity in Fig. 15(d) is greater than the simulated hydroplaning velocity mentioned, it is, therefore, observed that the water fluid enters most of the contact region between tire tread and road surface. At 0.120 s after tire entering the water film, the fluid flow velocity reaches 120 km/hr, and Fig. 15(e) shows the bottom view of the simulated splashing graph for this velocity condition. Note that the initial contact region is totally intruded by the water fluid, the tire seems to be completely lifted by the water fluid beneath the tire. In addition, the normal contact force at this moment descends to zero and the tire is floating on top of fluid water film. It means that a thin gap is generated between the tire and the road surface, no normal contact force exits. Keep in mind that a 25˚C water viscosity [Fox et al (2004)] of 8.93 x 10^{-4} N?s/m^2 was considered in the current fluid-structure interaction (FSI) FEM hydroplaning analysis.

Table 1: A comparison of the experimental result [Okano and Koishi (2001)] and codes simulated hydroplaning velocity for the smooth (blank) tread pattern 195/65R15 tire.

Tire tread pattern	Experiments	LS-DYNA Simulation
Smooth	69.3* (77.0**) km/hr	60.6* km/hr

* stands for the computed velocity of tire (Vt) base on the equation: s=1-(Vt/Vv), where s and Vv are the slip ratio of a tire and the measured vehicle velocity. Note that the slip ratio is set to be 10% based on the suggestion given by Okano and Koishi [Okano and Koishi (2001)].

** stands for the measured vehicle velocity.

Table 1 shows a comparison of the experimental result given by Okano and Koishi [Okano and Koishi (2001)] and the present LS-DYNA codes simulated hydroplaning tire velocity for a 195/65R15 smooth (blank) tread pattern tire. Note that the test determined vehicle hydroplaning velocity for this smooth pattern tire was reported to be 77.0 km/hr given by ref. [Okano and Koishi (2001)]. This velocity can be transformed to the hydroplaning tire velocity (V_t) using the equation suggested in ref. [Okano and Koishi (2001)] as: s = 1-(V_t/V_v), where "s" and "V_v" are, respectively, the slip ratio of a tire and the measured vehicle hydroplaning velocity.The

slip ratio is set to be 10% as suggested in ref. [Okano and Koishi (2001)]. Therefore, the hydroplaning tire velocity (V_t) derived from their test measured vehicle hydroplaning velocity of 77 km/hr for a 195/65R15 smooth tread pattern tire was calculated to be equal to 69.3 km/hr. The corresponding simulated hydroplaning tire velocity for the same smooth tire was already determined to be 60.6 km/hr using the present LS-DYNA fluid-structure interaction hydroplaning analysis. Limited difference between the present simulated smooth tread pattern hydroplaning tire velocity (i.e., 60.6 km/hr) and that derived by Okano and Koishi [Okano and Koishi (2001)] (i.e., 69.3 km/hr) is reported to be approximately 12.6 %. The deviation may be resulted from the variation of the material properties used in FEM simulations and the tire reported in ref. [Okano and Koishi (2001)].

5 Effect of the logitudinally grooved tread pattern on the hydroplaning characteristics

In addition to the hydroplaning analysis for smooth (blank) tread pattern tire reported in the previous section, tires with longitudinally-grooved tread pattern may influence their hydroplaning characteristics/performance. In the current study, two types of longitudinally-grooved tread pattern tires, i.e. the 9 mm narrow groove width type and the 18 mm wide groove width type, with a groove depth of 8 mm and two grooves 60 mm apart were numerically analyzed in order to examine their respective hydroplaning behavior. The Hypermesh pre-processor was also adopted to construct the 195/65R15 tire model with the specified tread patterns. Similar to the loading applied to the smooth tread pattern tire mentioned in the last section, the inflation pressure and also the vertical car weight are initially applied in 1 sec. and then tire rolls into the 10 mm thick water fluid film for 0.12 sec. physical time. It is designed that at the end of 1.12 sec. (i.e. the summation of 1 sec. and 0.12 sec.), the tire with longitudinally-grooved tread pattern is 200 kPa inflated, 4,000 N car weight loaded and rolls into the water film with a water fluid velocity of 120 km/hr. It is noted that the LS-DYNA section property of the 1 point integration with single material and void (SMV) options was chosen for the present water fluid film elements. In addition, both the dynamic and static friction coefficients were assumed to be 1.0 in the present numerical model. Fig. 16 shows the geometrical graphs of two longitudinally-grooved tread pattern tires with (a) 9 mm narrow groove width and (b) 18 mm wide groove width. There are 36,000 hexahedron & pentahedron solid and shell elements constructed for either the 9 mm narrow groove width or the 18 mm wide groove width tire model. Similar computational procedures using the LS-DYNA coupled code were used to solve the hydroplaning problem for the longitudinally-grooved tires rolling on a flat pavement with a 10 mm thick water fluid film.

Figure 16: The geometrical graphs of two longitudinally-grooved tread pattern tires with (a) 9 mm narrow groove width and (b) 18 mm wide groove width.

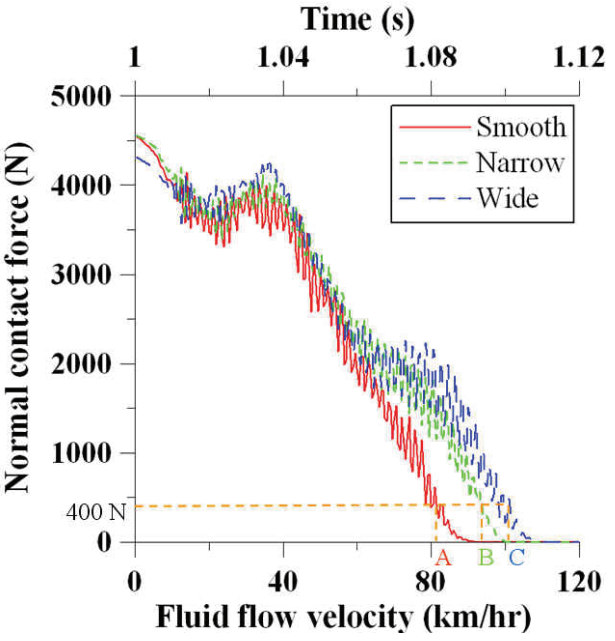

Figure 17: Relationship between normal contact force and fluid flow velocity established by using the ALE formulations for tire with prescribed tread patterns rolling over a 10 mm thick water film.

Fig. 17 shows the relationship between normal contact force and fluid flow velocity for the inflated tires with (1) smooth (blank) tread pattern, (2) 9 mm narrow longitu-

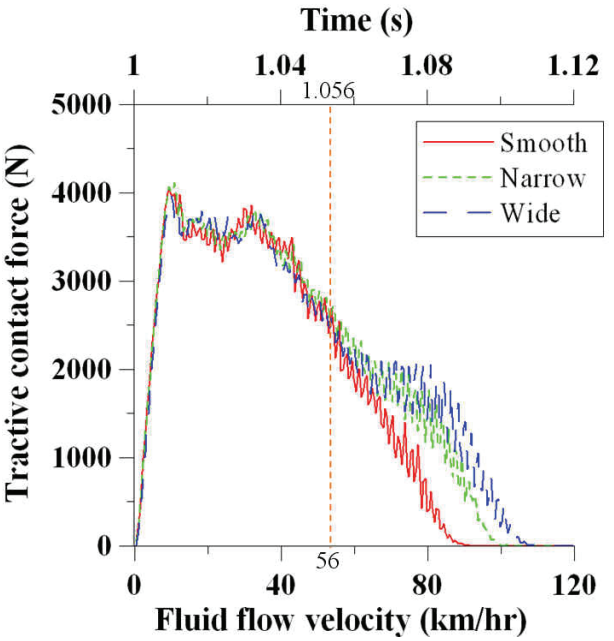

Figure 18: Relationship between tractive contact force and time after tire inflation and car weight loaded.

dinal grooved tread pattern, and (3) 18 mm wide longitudinal grooved tread pattern rolling over a 10 mm thick water film. Upon examining intersection points A, B and C shown in Fig. 17, it reveals that the fluid flow velocities corresponding to the hydroplaning behavior (i.e., 10% of the vertical car weight loading) were determined approximately to be 83, 94, and 101 km/hr for the smooth tire tread pattern, the 9 mm narrow longitudinally-grooved tire tread pattern, and the 18 mm wide longitudinally-grooved tire tread pattern, respectively. It is, furthermore, concluded that the 18 mm wide longitudinally-grooved tread pattern tire possesses the highest hydroplaning velocity in comparison with that of the smooth tread pattern tire and the 9 mm narrow longitudinally-grooved tread pattern tire. The wider the groove width of the longitudinally-grooved pattern tire may possess better hydroplaning velocity. Moreover, at higher fluid flow velocities, the curves shown in Fig. 17 deviate more clearly because of the variation of tire tread patterns introduced.

The relationship between the tire tractive (along vehicle traveling direction or y-direction) contact force and time for the hydroplaning analysis is presented in Fig. 18 for the (1) smooth (blank) tread pattern, (2) 9 mm narrow longitudinally-grooved tread pattern, and (3) 18 mm wide longitudinally-grooved tread pattern tires. Note

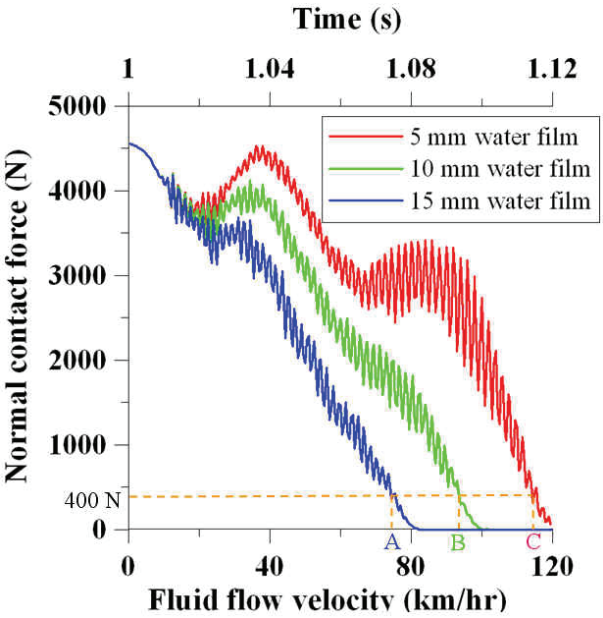

Figure 19: The relationship between normal contact force and hydroplaning velocity established by using Eulerian formulations for tire with 9 mm narrow longitudinal groove pattern.

that the starting time in Fig. 18 is equal to 1 sec. Because the tires studied here were 200 kPa inflated and 4,000 N car weight loaded from 0 sec to 1 sec. After 1 sec, the inflated tire starts to roll on a flat pavement with a water film of 10 mm thick for hydroplaning analysis. When the fluid flow velocity is greater than 56 km/hr (for time greater than 1.056 sec. as shown in Fig. 18), the tractive (y-direction) contact force curves deviate from one another more clearly for these three types of tires studied here. And this deviation is resulted from the variation of the tire tread patterns introduced. Note that when time is equal to 1.12 sec., it corresponds to a fluid flow velocity of 120 km/hr as shown in Fig. 18. The tractive contact forces for tires with smooth tread pattern and 9mm narrow and 18 mm wide longitudinally-grooved patterns are reported to be zero when the fluid flow velocity is about 120 km/hr (i.e., time equals to 1.12 sec.). Based on the present coupled FEM hydroplaning simulated results, the effect of longitudinally-grooved tread pattern on the hydroplaning velocity for a 195/65R15 radial tire studied could not be neglected. The fluid flow velocities corresponding to the hydroplaning behavior are reported to be approximately 83, 94, and 101 km/hr for the smooth tread pattern, the 9 mm narrow

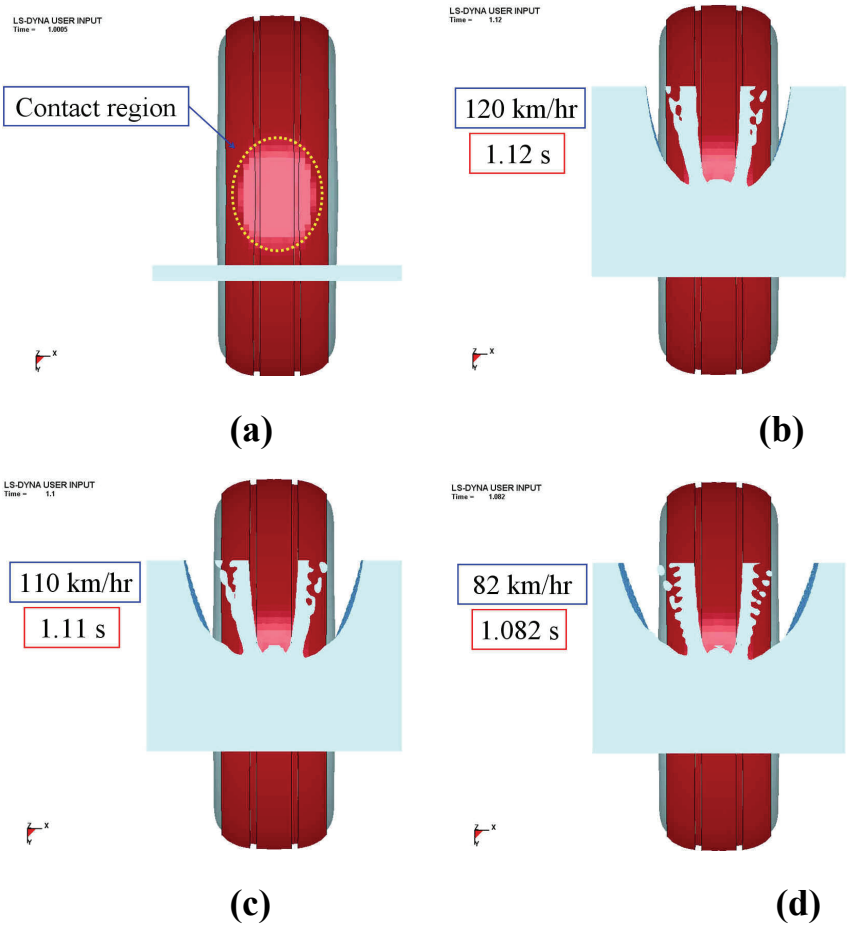

Figure 20: The bottom view of the simulated graphs for the 9 mm narrow longitudinal grooved tread pattern tire rolling over a water film when tire was accelerated from rest to a speed of (a) contact region and (b) 120 km/hr, (c) 110 km/hr, and (d) 82 km/hr.

longitudinally-grooved tread pattern, and the 18 mm wide longitudinally-grooved tread pattern tires, respectively. A 21.7% increase on the simulated hydroplaning velocity of the 18 mm wide longitudinally-grooved tread pattern tire is determined when compared with that of the tire with a smooth tread pattern.

6 Effect of various water/void layer thickness on the hydroplaning characteristics

Effect of the thickness of various water fluid film/void layer on the hydroplaning characteristics of a 9 mm narrow longitudinally-grooved tread pattern 195/65R15 tire are studied in this section. The 5, 10 and 15mm thickness of the water fluid film/void layers were constructed in the present fluid-structure interaction (FSI) FEM models. This coupled FEM model for tire hydroplaning analysis contains 109,560 hexahedron elements that were utilized to construct the water film and air void layers. The LS-DYNA code was used to analyze this coupled hydroplaning problem for a longitudinally-grooved tread pattern tire subjected to a 200 kPa inflation pressure loading and a 4,000 N car weight numerically loaded initially within 1 sec. This specific tire was then driven by the roadway and the fluid film. The velocity of the road and fluid film were increased from rest initially to 120 km/hr at the end with a constant acceleration in 0.12 s of the physical time as mentioned before. Fig. 19 shows the relationship between the normal contact force and fluid flow velocity for the inflated tire with 9 mm narrow longitudinally-grooved tread pattern tire rolling over 5, 10 and 15 mm thick water film from 1 sec. to 1.12 sec. of the physical time. Based on the A, B and C intersection points of the horizontal dotted line and three curves shown in Fig. 19, the simulated hydroplaning velocities corresponding to these three water film thickness were respectively determined to be 75, 93 and 114 km/hr. When the water fluid film/void layer thickness is increased from 5 mm to 15 mm, Fig. 19 reveals that a 34.2% decrease of the hydroplaning velocity was reported. The Arbitrary Lagrangian & Eulerian (ALE) formulation was adopted in the current numerical analysis. It is noted that the LS-DYNA section property of the 1 point integration with single material and void (SMV) options was chosen for the present water fluid film elements. Note also that the static and dynamic friction coefficients were set equal to one here.

Figures 20(a) shows a bottom view graph for a 9 mm narrow longitudinally-grooved tread pattern tire before rolling over a water film. The contact region between the tire tread and the dry road surface is shown in Fig. 20(a) when tire was 200 kPa pressure inflated and 4,000 N car weight loaded. Figures 20(b) to (d) show the bottom view of the simulated splashing graphs for a 9 mm narrow longitudinally-grooved tire rolling over a water film with a thickness of 5, 10 and 15 mm when the normal contact force between tire and roadway is zero. Figures 20(b) to (d), respectively, show the water fluid flow accelerated to velocities near 120 km/hr (0.12 s after acceleration initiated), 110 km/hr (0.11 s after acceleration initiated) and 82 km/hr (0.082 s after acceleration initiated). Notice that the hydroplaning velocities (i.e., 75, 93 and 114 km/hr) for these tires reported in the previous section are lower than the fluid flow velocity mentioned here. Because “hydroplaning velocity” was

previously defined as the transverse velocity at which the contact force between the tire and road surface drop to 10% of the tire load. Fig. 20(b) to (d) reveals that the thickness of water film on top of a road surface may affect a 9 mm narrow longitudinally-grooved tread pattern tire's hydroplaning characteristics clearly based on the current coupled FEM simulation result. It is concluded that a variation of the water film thickness can directly affect the hydroplaning performance of the 9 mm narrow longitudinally-grooved tread pattern tire.

7 Conclusions

Current work is concerned with the transient hydroplaning behavior of the inflated pneumatic automotive tires with various types of tread patterns. Tires were numerically loaded with a quarter car weight, and then accelerated from rest rolling over a water film with a thickness of 5, 10 and 15 mm on top of a flat pavement. The tire hydroplaning phenomenon was analyzed by the commercial finite element code - LS-DYNA. The Arbitrary Lagrangian & Eulerian (ALE) formulation was adopted to depict the fluid-structure interaction (FSI) behavior. Three different tire tread patterns, i.e. the smooth (blank) tread pattern and the 9 and 18 mm wide longitudinally-grooved tread patterns, were constructed to perform the present transient hydroplaning analysis. The previous MSC.Dytran coupled tire and fluid model reported by Okano and Koishi [Okano and Koishi (2001)] for hydroplaning characteristics analysis was reconstructed and performed using the Hypermesh pre-processor and the LS-DYNA solver. Limited difference (approximately 12.6%) between the present simulated smooth tread pattern hydroplaning tire velocity (i.e., 60.6 km/hr) and that derived by Okano and Koishi [Okano and Koishi (2001)] (i.e., 69.3 km/hr) is reported. The deviation may be resulted from the variation of the material properties used in FEM simulations and the tire reported in ref. [Okano and Koishi (2001)]. Therefore, the present analysis scheme seems to be accurate and adequate for the current tire rolling and hydroplaning FSI coupled analysis. Two types of longitudinally-grooved tires, i.e. the 9 mm narrow groove width type and the 18 mm wide groove width type, with groove depth of 8 mm and two grooves 60 mm apart were numerically analyzed in order to examine their respective hydroplaning behavior. The fluid flow velocities corresponding to the hydroplaning behavior were determined to be 83, 94, and 101 km/hr for the smooth tire tread pattern, the 9 mm narrow longitudinally-grooved tire tread pattern, and the 18 mm wide longitudinally-grooved tread tire pattern, respectively. It is, furthermore, concluded that the 18 mm wide longitudinally-grooved tread pattern tire possesses the highest hydroplaning velocity in comparison with that of a smooth tread pattern tire and a 9 mm narrow longitudinally-grooved tread pattern tire. A 21.7% increase on the simulated hydroplaning velocity of the 18 mm wide longitudinally-grooved

tread pattern tire is reported when compared with that of a smooth tread pattern tire. Furthermore, the effect of various water fluid film/void layer thickness on the hydroplaning characteristics for a 9 mm narrow longitudinally-grooved tread pattern 195/65R15 tire were also reported. The 5, 10 and 15 mm thickness of the water fluid film/void layers were constructed in the present fluid-structure interaction (FSI) FEM models. The simulated hydroplaning velocities corresponding to these three water film thickness were respectively determined to be 75, 93 and 114 km/hr. When the water fluid film/void layer thickness is increased from 5 mm to 15 mm, a 34.2% decrease of the hydroplaning velocity is reported.

Acknowledgement: The authors would like to thank the National Science Council (NSC), Taiwan, R.O.C. for supporting this work under contract no. NSC 97-2221-E-006-053-MY2 and also the Cheng Shin Rubber Ind. Co. Ltd. for their previous partial financial support under a cooperative research project during 2006-2007.

References

An J. C., Cho J. R. (2008): Tire standing wave simulation by 3-D explicit finite element method, ICCES, v. 7(3), pp. 123-128.

Clark S. K. (1981): Mechanics of pneumatic tires, US Department of Transportation, Washington, DC, USA.

Fox R. W., McDonald A. T., Pritchard P. J. (2004): Introduction to Fluid Mechanics, 6th Edition, John Wiley & Sons, Inc., Hoboken, NJ, USA.

Ghoreishy M. H. R. (2006): Steady state rolling analysis of a radial tyre: comparison with experimental results, Journal of Automobile Engineering, 220(6), pp. 713-721.

Gibson R. F. (2007): Principles of Composite Material Mechanic, 2nd Edition, CRC Press, Taylor & Francis Group, LLC, Boca Raton, FL, USA.

Grogger H., Weiss M. (1996): Calculation of the Three-Dimensional Free Surface Flow Around and Automobile Tire, Tire Science and Technology TSTCA, 24(1), pp. 39-49.

Grogger H., Weiss M. (1997): Calculation of the Hydroplaning of a Deformable Smooth-Shaped and Longitudinally-Grooved Tire, Tire Science and Technology TSTCA, 25(4), pp. 265-287.

Jenq S. T., Chiu Y. S., Ting Y. C., Chu C. (2008): Dynamic Contact Rolling Analysis for Tires with Smooth and Longitudinal grooved Tread Patterns Passing a Speed Bump Obstacle, the Proceedings of the 3rd International Symposium on Advanced Fluid/Solid Science and Technology in Experimental Mechanics (ISEM 2008), Tainan, Taiwan, ROC.

Jenq S. T., Ting Y. C., Liang S. M., Lin D., Shih M. (2008): Quasi-static compression and rolling contact analysis of MAXXIS VICTRA MA-Z1 tire on dry roadway, International Journal of Modern Physics B, 22(9/11), pp. 1531-1537.

Nakajima Y., Seta E., Kamegawa T., Ogawa H. (2000): Hydroplaning Analysis by FEM and FVM: Effect of Tire Rolling and Tire Pattern on Hydroplaning, *International Journal of Automotive Technology*, 1(1), pp. 26-34.

Okano T., Koishi M. (2001): A New Computational Procedure to Predict Transient Hydroplaning Performance of a Tire, Tire Science and Technology TSTCA, 29(1), pp. 2-22.

Reaz Ahmed S., Deb Nath S. K. (2009): A simplified analysis of the tire-tread contact problem using displacement potential based finite-difference technique, *CMES: Computer Modeling and Engineering Science*, v. 44(1), pp. 35-63.